

• Original Paper •

Ensemble Forecasts of Tropical Cyclone Track with Orthogonal Conditional Nonlinear Optimal Perturbations

Zhenhua HUO^{1,2}, Wansuo DUAN^{*2,3}, and Feifan ZHOU^{3,4}

¹National Meteorological Center, China Meteorological Administration, Beijing 100081, China

²State Key Laboratory of Numerical Modeling for Atmospheric Sciences and Geophysical Fluid Dynamics, Institute of Atmospheric Physics, Chinese Academy of Sciences, Beijing 100029, China

³University of Chinese Academy of Sciences, Beijing 100049, China

⁴Laboratory of Cloud-Precipitation Physics and Severe Storms, Institute of Atmospheric Physics, Chinese Academy of Sciences, Beijing 100029, China

(Received 9 January 2018; revised 13 September 2018; accepted 9 October 2018)

ABSTRACT

This paper preliminarily investigates the application of the orthogonal conditional nonlinear optimal perturbations (CNOPs)–based ensemble forecast technique in MM5 (Fifth-generation Pennsylvania State University–National Center for Atmospheric Research Mesoscale Model). The results show that the ensemble forecast members generated by the orthogonal CNOPs present large spreads but tend to be located on the two sides of real tropical cyclone (TC) tracks and have good agreements between ensemble spreads and ensemble-mean forecast errors for TC tracks. Subsequently, these members reflect more reasonable forecast uncertainties and enhance the orthogonal CNOPs–based ensemble-mean forecasts to obtain higher skill for TC tracks than the orthogonal SVs (singular vectors)–, BVs (bred vectors)– and RPs (random perturbations)–based ones. The results indicate that orthogonal CNOPs of smaller magnitudes should be adopted to construct the initial ensemble perturbations for short lead–time forecasts, but those of larger magnitudes should be used for longer lead–time forecasts due to the effects of nonlinearities. The performance of the orthogonal CNOPs–based ensemble-mean forecasts is case-dependent, which encourages evaluating statistically the forecast skill with more TC cases. Finally, the results show that the ensemble forecasts with only initial perturbations in this work do not increase the forecast skill of TC intensity, which may be related with both the coarse model horizontal resolution and the model error.

Key words: ensemble forecast, initial perturbation, conditional nonlinear optimal perturbation, tropical cyclone

Citation: Huo, Z. H., W. S. Duan, and F. F. Zhou, 2019: Ensemble forecasts of tropical cyclone track with orthogonal conditional nonlinear optimal perturbations. *Adv. Atmos. Sci.*, **36**(2), 231–247, <https://doi.org/10.1007/s00376-018-8001-1>.

1. Introduction

For numerical atmospheric and oceanic forecast systems, model errors and initial errors always exist. Due to the instability of atmospheric and oceanic systems and their related nonlinearities, small initial errors may grow nonlinearly and lead to large forecast errors (Lorenz, 1963). Ensemble forecasting techniques have been an effective and popular way to estimate and reduce forecast errors in operational forecasts. The basic idea of ensemble forecasting was proposed by Leith (1974), who specifically proposed the Monte Carlo Forecasting method (also known as the random perturbations method; hereafter denoted as the RPs method) to estimate the probability distribution function of forecast results. For the RPs method, random perturbations are superimposed on the initial analysis field to generate a group of forecast members.

These forecast members can be used to estimate the uncertainties of forecast results and calculate the occurrence probability for the weather or climate events of concern. Leith (1974), Molteni et al. (1996), Buizza et al. (2005), and Leutbecher and Palmer (2008) have indicated that the average of the ensemble forecast members, i.e., the ensemble mean, may leave the common predictable parts and filter out the unpredictable parts of the forecast members, which ultimately decreases the uncertainties of the single and deterministic forecast result.

In recent years, several methods have been developed to produce the initial perturbations and adopted in different operational centers for operational ensemble forecasts. For example, the singular vectors (SVs) method proposed by Lorenz (1965) has been successfully applied in the ECMWF (European Centre for Medium-Range Weather Forecasts) for operational ensemble forecasts (Mureau et al., 1993; Molteni et al., 1996). SVs are initial perturbations that are orthogonal and have the largest linear growth rates in their respective

* Corresponding author: Wansuo DUAN
Email: duanws@lasg.iap.ac.cn

subspaces of initial perturbations during the optimization period. Though SVs have been successfully applied in operational centers for ensemble forecasts, there also exist some limitations for SVs. Gilmour and Smith (1998) noted that the SVs method has limitations in the construction of initial ensemble perturbations because of the linear approximation of the SVs method. Anderson (1997) indicated that in a linear regime SVs are effective to grasp the fast growing initial perturbations, but in nonlinear regimes SVs cannot describe the extreme perturbations well. All these aspects may limit the benefits of SVs for improving ensemble forecast skill.

In view of the limitations of SVs in nonlinear regimes, Mu et al. (2003) proposed the conditional nonlinear optimal perturbation (CNOP) method. Duan et al. (2004) showed that the CNOP represents the initial perturbation that has the largest nonlinear evolution at a given forecast time among all the initial perturbations that satisfy a certain physical constraint [also see Mu and Zhang (2006) and Duan and Mu (2009)]. As the leading SV (LSV) is the initial perturbation that has the largest growth rate in a linear regime, CNOP can be regarded as the nonlinear extension of the LSV. In consideration of the impact of nonlinearity on ensemble forecasts, Mu and Jiang (2008) replaced the LSV with CNOP, while keeping other SVs unchanged, to obtain the initial perturbations of ensemble forecasts with a two-dimensional barotropic quasi-geostrophic model. The obtained results showed that the ensemble forecast skill had been improved [also see Jiang and Mu (2009)]. This indicates that it is useful and important in ensemble forecasting to find those initial perturbations that have large nonlinear evolutions. However, in the approach suggested by Mu and Jiang (2008), other SVs that develop optimally only in a linear regime still exist.

To fully consider the effects of nonlinearities, Duan and Huo (2016) proposed the method of orthogonal CNOPs and applied it to yield ensemble forecast initial perturbations by using the Lorenz-96 model (Lorenz, 1995). They showed that the orthogonal CNOPs overcome the limitations of SVs, guarantee the diversity of ensemble members and effectively estimate the initial uncertainties of forecasts, making the associated ensemble forecasts more skillful than those associated with the orthogonal SVs. However, such results are derived from the simple Lorenz-96 model and are therefore only generally indicative. To be more realistic, we should adopt a more complete model to explore the usefulness of the orthogonal CNOPs in ensemble forecasts. Therefore, we may naturally ask whether the orthogonal CNOPs behave better than the orthogonal SVs in ensemble forecasts with more complex weather models, such as the Fifth-generation Pennsylvania State University–National Center for Atmospheric Research Mesoscale Model (MM5; Dudhia, 1993; Grell et al., 1994) or the Weather Research and Forecasting Model (WRF; Skamarock et al., 2005). In addition, there are other methods of generating initial perturbations for ensemble forecasts, such as the bred vectors [BVs; see next section; also see Toth and Kalnay, 1993, 1997] and the abovementioned RPs. Is the orthogonal CNOPs method also more advanced than these two methods?

To answer the above questions, we adopt MM5 to conduct ensemble forecasting experiments, and use the above methods to generate the initial perturbations for the ensemble forecasts. Although the MM5 model seems a little outdated, it possesses effective tangent-linear and adjoint models (Zou et al., 1997) and provides a way to efficiently compute SVs and CNOPs. Furthermore, MM5 and its tangent-linear and adjoint models have been widely applied in studies of data assimilation, ensemble forecasts and the related predictabilities of extreme weather events, such as tropical cyclones (TCs) and heavy rain (Cheung, 2001; Chien and Jou, 2004; Liang et al., 2007; Mu et al., 2009; Pessi and Businger, 2009; Hwang et al., 2011; Wei, 2012; Yang et al., 2012; Zhao et al., 2012; Yu et al., 2017). Those studies adopted MM5 to either explore the predictability dynamics of related weather events or to act as a platform to examine the usefulness of new approaches. For example, Mu and colleagues recently used MM5 and its tangent and adjoint models to examine the feasibility of the CNOP approach in revealing the predictability of TCs (Mu et al., 2009; Qin and Mu, 2011; Zhou and Mu, 2011; Jiang and Wang, 2012; Qin et al., 2013; Mu et al., 2014; Yu et al., 2017). Therefore, it is acceptable for us to regard MM5 as a platform to examine the usefulness of the orthogonal CNOPs in yielding initial perturbations and improving the ensemble forecast skill.

Considering TC-induced severe disasters, we follow these previous studies and continue to use TC predictability as the point of interest to examine the performance of orthogonal CNOPs in the ensemble forecasts (especially using a complex model) and the superiority of orthogonal CNOPs to other methods. As we know, due to the lack of conventional observational data over the tropical ocean, the initial-value problem has become a key question for TC-track forecasts. Furthermore, previous studies have shown that TC-track forecasts are very sensitive to initial states (Langland et al., 2002; Hsiao et al., 2009; Yamaguchi et al., 2012). Particularly, Yamaguchi et al. (2009) demonstrated that the ensemble forecasts associated with initial perturbations improve the TC-track forecast skill. Zhang and Krishnamurti (1997) and Cheung (2001) also obtained similar results. Therefore, we follow these works and regard the TC-track forecast as an initial value problem to examine the skill of the ensemble forecasts generated by the orthogonal CNOPs.

The paper is organized as follows: The model (MM5) and the selected TC cases are introduced in section 2. The orthogonal CNOPs– and SVs–, RPs– and BVs–based methods are described in section 3. In section 4, the ensemble forecasting experiments for TC tracks conducted by using orthogonal CNOPs–, orthogonal SVs–, RPs–, and BVs–based ensemble forecast techniques are described and the related forecast skills are subsequently compared. Then, the results are discussed in section 5 and a summary is provided in section 6.

2. MM5 and the TC cases

MM5 (Dudhia, 1993; Grell et al., 1994) is a mesoscale model developed by the National Center for Atmo-

spheric Research and Pennsylvania State University. It is a non-hydrostatic, limited-area, terrain-following sigma (σ)-coordinate model, and was designed to simulate and predict mesoscale atmospheric circulations (Dudhia, 1993; Grell et al., 1994). MM5 was also employed in Mu et al. (2014), and the following text is taken from there with some modifications. The horizontal resolution (dx) of the model used here is 60 km, with the model domain covering 51×61 (y -direction by x -direction) grid points. The vertical direction is evenly divided into 20 σ levels, and the integration time step is in seconds chosen on the basis of the $3 \times dx$ criterion. Following Mu et al. (2009) and Zhou and Mu (2011, 2012), the physical parameterizations associated with the TC simulations include the Anthes–Kuo cumulus parameterization scheme, the simple cooling radiation scheme, the high-resolution Blackadar planetary boundary layer parameterization scheme, and the stable precipitation scheme. Since MM5 is a regional model, it requires not only an initial condition but also a boundary condition. The initial and boundary conditions used here are supplied by interpolating the National Centers for Environmental Prediction (NCEP) FNL (Final) Operational Global Analysis ($1^\circ \times 1^\circ$) into MM5 grids. Integrating MM5 with the initial and boundary conditions, one can obtain a control forecast for weather events of concern.

The historical TC data, i.e., the best-track data, adopted in the present study, are available online at http://tcdata.typhoon.org.cn/en/zjljsjj_zlhq.html [also see Ying et al. (2014)]. We select five TCs to study the ensemble forecasts associated with orthogonal CNOPs. The five TCs are the severe typhoon (STY) Matsa (2005), severe tropical storm (STS) Bilis (2006), super typhoon (Super TY) Sepat (2007), typhoon (TY) Morakot (2009), and STS Fungwong (2014). These TCs were of different intensity but all made landfall in China and caused severe disasters. Table 1 shows the model domain center, the forecast periods, the minimum sea level pressure at the initial time, the maximum wind speed at the initial time, and the initial intensity category for each of the five TCs. The TC intensity category is divided based on the maximum wind speed, and the TC intensity category standard is available online at http://tcdata.typhoon.org.cn/en/zjljsjj_sm.html [also see General Administration of Quality Supervision, Inspection and Quarantine of the People’s Re-

public of China and Standardization Administration of the People’s Republic of China (2006)]. Here, the model domains for each TC are selected to cover the TC tracks during the forecast period. The forecast periods are chosen as five days for the first four TCs in Table 1, but four days for the last TC case (which decayed after four days’ evolution). Note that the forecast period for each TC covers its landing process.

3. The orthogonal CNOPs, SVs, RPs, and BVs

In the present study, the orthogonal CNOPs are used to generate ensemble initial perturbations for the TC tracks. The related forecast skills are compared with those associated with the orthogonal SVs, RPs, and BVs methods. Integrating MM5 with the initial and boundary conditions derived from the FNL data, we can derive the control forecast. We use each method to experimentally generate five initial perturbations for one TC, and then add them to and subtract them from the initial analysis to obtain 10 perturbed initial conditions. The control forecast can be obtained by integrating MM5 with the unperturbed initial analysis field. Then, integrating MM5 with these perturbed initial conditions, we can obtain 10 perturbed forecast members for the TC case. Therefore, there are 11 ensemble forecast members in total for each TC and each method. Using the resultant ensemble members, the skills of ensemble forecasts can be evaluated and a comparison among the aforementioned methods realized.

3.1. Orthogonal CNOPs

The orthogonal CNOPs method is the same as proposed and employed by Duan and Huo (2016). Specifically, orthogonal CNOPs are a group of nonlinear optimal initial perturbations denoted as 1st-CNOP, 2nd-CNOP, 3rd-CNOP, . . . , n th-CNOP. The 1st-CNOP is the nonlinear optimal initial perturbation that has the largest nonlinear evolution at the end of the optimization time period in the whole perturbation phase space Ω_1 . The j th-CNOP represents the nonlinear optimal initial perturbation in the subspace Ω_j that is orthogonal to 1st-CNOP, 2nd-CNOP, 3rd-CNOP, . . . , $(j - 1)$ th-CNOP. In present study, the j th-CNOP can be defined as the initial perturbation $\mathbf{x}_{0,j}^*$, which satisfies the following optimization

Table 1. The model domain center, forecast period (UTC), minimum sea level pressure at the initial time, maximum wind speed at the initial time, and initial intensity category for each of the five typhoon cases.

Case	Domain center	Forecast period	Minimum sea level pressure	Maximum wind speed	Initial intensity category
STY Matsa (2005)	(28°N, 122°E)	1200 UTC 3 August 2005 to 1200 UTC 8 August 2005	960 hPa	40 m s ⁻¹	TY
STS Bilis (2006)	(22°N, 122°E)	1200 UTC 10 July 2006 to 1200 UTC 14 July 2006	990 hPa	23 m s ⁻¹	TS
Super TY Sepat (2007)	(21°N, 123°E)	1200 UTC 15 August 2007 to 1200 UTC 20 August 2007	935 hPa	55 m s ⁻¹	Super TY
TY Morakot (2009)	(23°N, 125°E)	0600 UTC 5 August 2009 to 0600 UTC 10 August 2009	975 hPa	33 m s ⁻¹	TY
STS Fungwong (2014)	(26°N, 121°E)	0000 UTC 19 September 2014 to 0000 UTC 24 September 2014	995 hPa	20 m s ⁻¹	TS

problem:

$$\begin{aligned} J(\mathbf{x}_{0,j}^*) &= \max_{\mathbf{x}_{0,j} \in \Omega_j} J(\mathbf{x}_{0,j}) \\ &= \max_{\mathbf{x}_{0,j} \in \Omega_j} [M_\tau(\mathbf{X}_0 + \mathbf{x}_{0,j}) - M_\tau(\mathbf{X}_0)]^T \times \\ &\quad \mathbf{C}[M_\tau(\mathbf{X}_0 + \mathbf{x}_{0,j}) - M_\tau(\mathbf{X}_0)], \end{aligned} \quad (1)$$

where \mathbf{X}_0 , composed of zonal wind \mathbf{u} , meridional wind \mathbf{v} , temperature \mathbf{T} and surface pressure \mathbf{p}_s , is the initial condition of a reference state, where the reference state can be understood as a control forecast; $\mathbf{x}_{0,j}$ is the corresponding initial perturbation in the subspace Ω_j ; τ is the optimization time period; M_τ is the propagator of MM5; the superscript ‘‘T’’ is the transposition symbol; the objective function $J(\mathbf{x}_{0,j})$ evaluates the magnitude of the nonlinear evolution of the initial perturbation $\mathbf{x}_{0,j}$ at the end of the optimization time period τ , which is the dry energy of the nonlinear evolved perturbation; and \mathbf{C} is the operator corresponding to the dry energy norm, which satisfies:

$$\delta \mathbf{X}^T \mathbf{C} \delta \mathbf{X} = \frac{1}{D} \int_D \int_0^1 \left[\mathbf{u}'^2 + \mathbf{v}'^2 + \frac{c_p}{T_r} \mathbf{T}'^2 + R_a T_r \left(\frac{\mathbf{p}'_s}{p_r} \right)^2 \right] d\sigma dD, \quad (2)$$

where the perturbation vector $\delta \mathbf{X}$ is composed of the perturbed zonal wind \mathbf{u}' , the perturbed meridional wind \mathbf{v}' , the perturbed temperature \mathbf{T}' and the perturbed surface pressure \mathbf{p}'_s . D is the horizontal domain, which corresponds to the operator \mathbf{C} , and σ represents the vertical coordinate. The constant $c_p = 1005.71 \text{ J kg}^{-1} \text{ K}^{-1}$ is the specific heat at a constant pressure, $R_a = 287.04 \text{ J kg}^{-1} \text{ K}^{-1}$ is the gas constant of the dry air, and $p_r = 1000 \text{ hPa}$ and $T_r = 270 \text{ K}$ are the reference parameters.

The subspace Ω_j is described by:

$$\Omega_j = \begin{cases} \{\mathbf{x}_{0,j} \in \mathbb{R}^n | \mathbf{x}_{0,j}^T \mathbf{C}_1 \mathbf{x}_{0,j} \leq \beta\}, & j=1 \\ \{\mathbf{x}_{0,j} \in \mathbb{R}^n | \mathbf{x}_{0,j}^T \mathbf{C}_1 \mathbf{x}_{0,j} \leq \beta, \mathbf{x}_{0,j} \perp \Omega_k, k=1, \dots, j-1\}, & j>1 \end{cases}, \quad (3)$$

where $\mathbf{x}_{0,j}$ is the initial perturbation, \mathbb{R} denotes the real number symbol, n is the vector dimension of $\mathbf{x}_{0,j}$, β is a positive number that limits the amplitudes of the initial perturbations with units of J kg^{-1} , and \mathbf{C}_1 is the operator corresponding to the initial dry energy norm. $\mathbf{x}_{0,j}^T \mathbf{C}_1 \mathbf{x}_{0,j}$ evaluates the magnitude of the initial perturbation, which is the dry energy of the initial perturbation corresponding to the whole model domain. Note that, when the objective function is defined to evaluate the dry energy for the evolved perturbations in the whole domain, there are always instabilities in the computation of CNOPs. Therefore, the initial perturbations $\mathbf{x}_{0,j}$ are produced over the whole model domain D_1 (\mathbf{C}_1 corresponds to D_1), but the objective function is defined to evaluate the dry energy in the remaining domain D by removing three grids near the boundary of the whole model domain (\mathbf{C} corresponds to D) to confirm the computational stability. Here, we use the SPG2 [Spectral Projected Gradient 2 (Birgin et al., 2000)] method to compute the j th-CNOP ($j = 1, 2, 3, \dots, n$) with the optimization time period τ being 24 h.

3.2. Orthogonal SVs, RPs, and BVs

The orthogonal SVs, RPs, and BVs methods are used in the same environment as that of the orthogonal CNOPs. In other words, the perturbed physical variables, the model domains and the norms to measure the perturbations are the same as those used for the orthogonal CNOPs.

According to the definition of orthogonal SVs, the cost function of SVs can be written as shown in Eq. (4), which measures the linear growth rates of the initial perturbations. Obviously, the orthogonal SVs represent the linear fastest-growing initial perturbations in their respective subspaces:

$$J(\mathbf{x}_0^*) = \max_{\mathbf{x}_0 \in \Omega} \frac{(\mathbf{L}\mathbf{x}_0)^T \mathbf{C}(\mathbf{L}\mathbf{x}_0)}{\mathbf{x}_0^T \mathbf{C}_1 \mathbf{x}_0}, \quad (4)$$

where \mathbf{x}_0 is the initial perturbation, $\Omega = \{\mathbf{x}_0 \in \mathbb{R}^n | \mathbf{x}_0^T \mathbf{C}_1 \mathbf{x}_0 \leq \beta\}$ is the constraint condition of the initial perturbations, and \mathbf{L} is the linear propagator of MM5. The SVs are computed using the Lanczos algorithm (Simon, 1984), with the optimization time period being 24 h, and are then scaled to match the magnitudes of the orthogonal CNOPs, which guarantees a fair comparison between the CNOPs and SVs.

For the RPs approach, the initial perturbations are random. Compared with the orthogonal CNOPs and SVs, the computations of RPs save computational resources and time, but RPs do not have specific dynamical significances, i.e., they could be either growing initial perturbations or decaying initial perturbations. The RPs are produced using the following steps: (i) subtract the initial analysis field from the forecast field of the control forecast at 24 h to get the error field \mathbf{E} ; (ii) for the components \mathbf{u}' , \mathbf{v}' , \mathbf{T}' and \mathbf{p}'_s in the error field \mathbf{E} , compute their maximum a and minimum b at each σ level; (iii) generate random numbers that obey the uniform distribution and belong to $[a, b]$, and then use them to create a random perturbation \mathbf{x}_0 with the components \mathbf{u}' , \mathbf{v}' , \mathbf{T}' and \mathbf{p}'_s ; (iv) scale the perturbation \mathbf{x}_0 so that it has the same magnitude as the orthogonal CNOPs. Using these steps, we get one RP. Repeating steps (iii) to (iv), we can get different RPs.

BVs, as mentioned above, are also used to generate ensemble forecasts. The performance of BVs is compared with that of the orthogonal CNOPs. In a data assimilation cycle, random errors may evolve in fast-growing directions in the atmospheric flow. According to this rationale, BVs are proposed to simulate the initial perturbations with fast-growing directions by periodically rescaling the differences between a set of forecasts and the corresponding perturbation forecasts. In this study, the components of the BVs are the same as in the above methods, i.e., the horizontal wind, meridional wind, temperatures and surface pressure. The norm to measure the initial perturbations and scale the perturbations is the same as that used for computing orthogonal CNOPs. The computation of the BVs starts 24 h ahead of the start time of the ensemble forecast, and the rescaling period is 6 h. Specifically, we add the RP obtained as described in the last paragraph to the initial analysis field of the control forecast to get the perturbed initial field. Integrating the perturbed initial field for 6 h, we can get the perturbed forecast. Subtracting

the control forecast from that of the perturbed forecast, we can get the error field. Second, we scale the error field so that it has the same magnitude as the orthogonal CNOPs. Then, we apply this scaled error field as the initial perturbation over the next 6-h integration. After four integrations, we can get the final scaled error field, i.e., the BV. Using different RPs, we can obtain different BVs that are used for ensemble forecasts.

4. Ensemble forecast experiments for the TC cases

In this section, we conduct ensemble forecast experiments of the selected five TC cases (see Table 1). As mentioned in section 2, these five TC cases had different intensities and all made landfall in China. Here, we investigate the ensemble forecast by calculating the mean of the ensemble forecast members of the TC track. In other words, we evaluate the forecast skill of the ensemble-mean forecast for the TC track, which is then compared with that of the control forecast to obtain the improvement in the ensemble-mean forecast. Here, the TC track is determined by the time-dependent TC center locations, which are identified by the locations where the sea level pressure is minimal. Usually, a better ensemble forecast system means that the ensemble forecast members' spreads should be closer to the ensemble-mean forecast errors (Branković et al., 1990; Eckel and Mass, 2005; Buckingham et al., 2010). Therefore, we also compute the ensemble forecast members' spreads and analyze the re-

lations between the ensemble-mean forecast errors and the ensemble spreads. The details for the calculations of the forecast error, ensemble spread, and improvement can be found in the Appendix.

The amplitudes of the initial perturbations of the ensemble forecast, which are limited by the constraint condition $\mathbf{x}_0^T \mathbf{C}_1 \mathbf{x}_0 \leq \beta$ in Eqs. (3) and (4), have been experimentally chosen as $\beta = 0.3 \text{ J kg}^{-1}$, $\beta = 0.3 \times 4 \text{ J kg}^{-1}$ and $\beta = 0.3 \times 9 \text{ J kg}^{-1}$. We use these constraint conditions to compute the orthogonal CNOPs and SVs. We find that the orthogonal CNOPs are more different from the orthogonal SVs when β is much larger. The differences between the CNOPs and SVs reflect the effects of nonlinearities. To better show the influences of nonlinearities on the ensemble forecasts, we present the results with $\beta = 0.3 \times 9 \text{ J kg}^{-1}$. The constraint condition of $\beta = 0.3 \times 9 \text{ J kg}^{-1}$ is physically reasonable. Pu et al. (1997) showed that the root-mean-square errors (RMSEs) of the temperature and wind of the FNL analysis field against the rawinsonde and dropsonde data at each vertical level are respectively smaller than approximately 3 K and 6 m s⁻¹. Eom and Myoung-Seok (2011) showed that the RMSEs of temperature and the zonal and meridional winds of FNL, when compared to the rawinsonde data at Osan and Gwangju from each vertical level, are less than 2 K, 3.5 m s⁻¹ and 3 m s⁻¹, respectively. Li et al. (2014) showed that the RMSEs of the temperature and wind speed of FNL against the observational data are smaller than approximately 2 K and 5.2 m s⁻¹, respectively, at each vertical level. In particular, they all showed that the RMSEs for wind approximately increase with vertical height. In Fig. 1, we show the vertical distri-

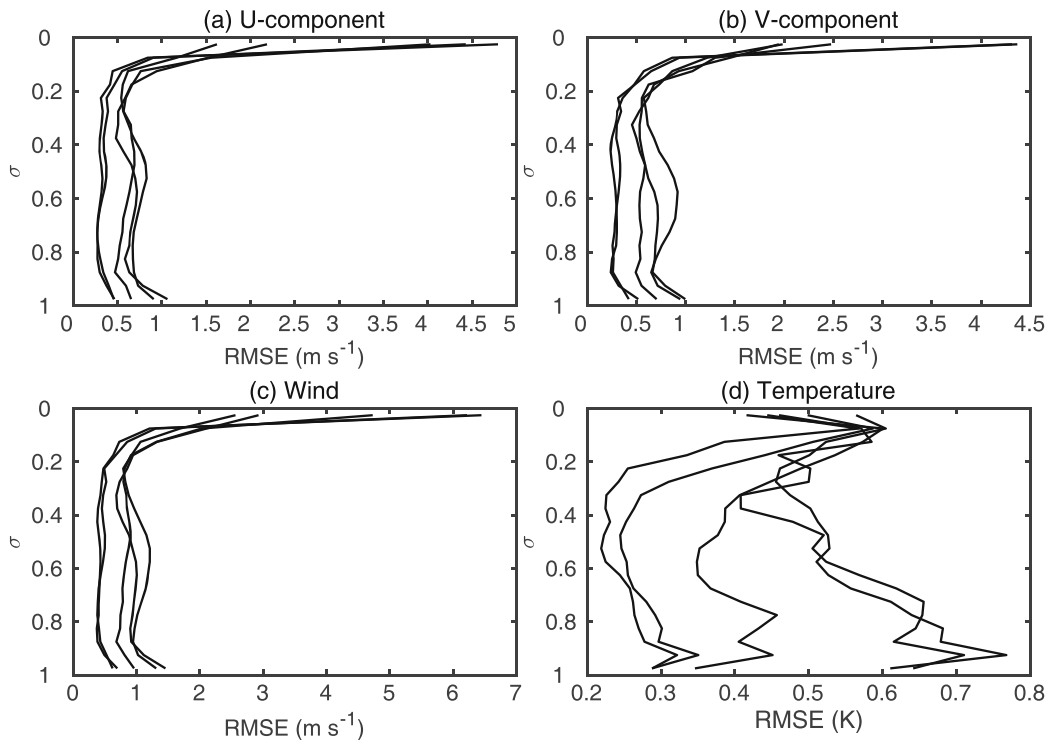


Fig. 1. Vertical distributions of the RMSEs of the (a) *U*-component, (b) *V*-component, (c) wind component, and (d) temperature component of the first five CNOPs for STY Matsa (2005) with $\beta = 0.3 \times 9 \text{ J kg}^{-1}$. The horizontal axis denotes the RMSE value and the vertical axis denotes the value of the vertical coordinate σ .

bution of the RMSE of the U - and V -wind speed and temperature components of the first five orthogonal CNOPs for STY Matsa (2005). It can be seen that the temperature, zonal and meridional winds and their related vertical structures of orthogonal CNOPs approximately satisfy the magnitudes and distributions of the analysis errors shown in Pu et al. (1997), Li et al. (2014) and Eom and Myoung-Seok (2011), with the largest RMSE of zonal wind, meridional wind, wind speed, and temperature being less than 5 m s^{-1} , 4.5 m s^{-1} , 6.5 m s^{-1} and 0.8 K , respectively. For the other TC cases, the related orthogonal CNOPs also show reasonable error distribu-

tion for their related variables, so the details are not shown here. Therefore, we choose $\beta = 0.3 \times 9 \text{ J kg}^{-1}$ to compute the orthogonal CNOPs, and the orthogonal SVs, BVs and RPs. Figure 2 plots the first five CNOPs, SVs, BVs, and RPs. It is shown that they present different patterns from each other. As a result, the skills of the ensemble forecasts may be different if the related initial perturbations are generated by these four methods. Therefore, which one would have higher forecast skill for the TC track? This is an issue we are interested in.

Figure 3 illustrates the forecast and observed tracks of the five TC cases. It is shown that the TC tracks for the orthogo-

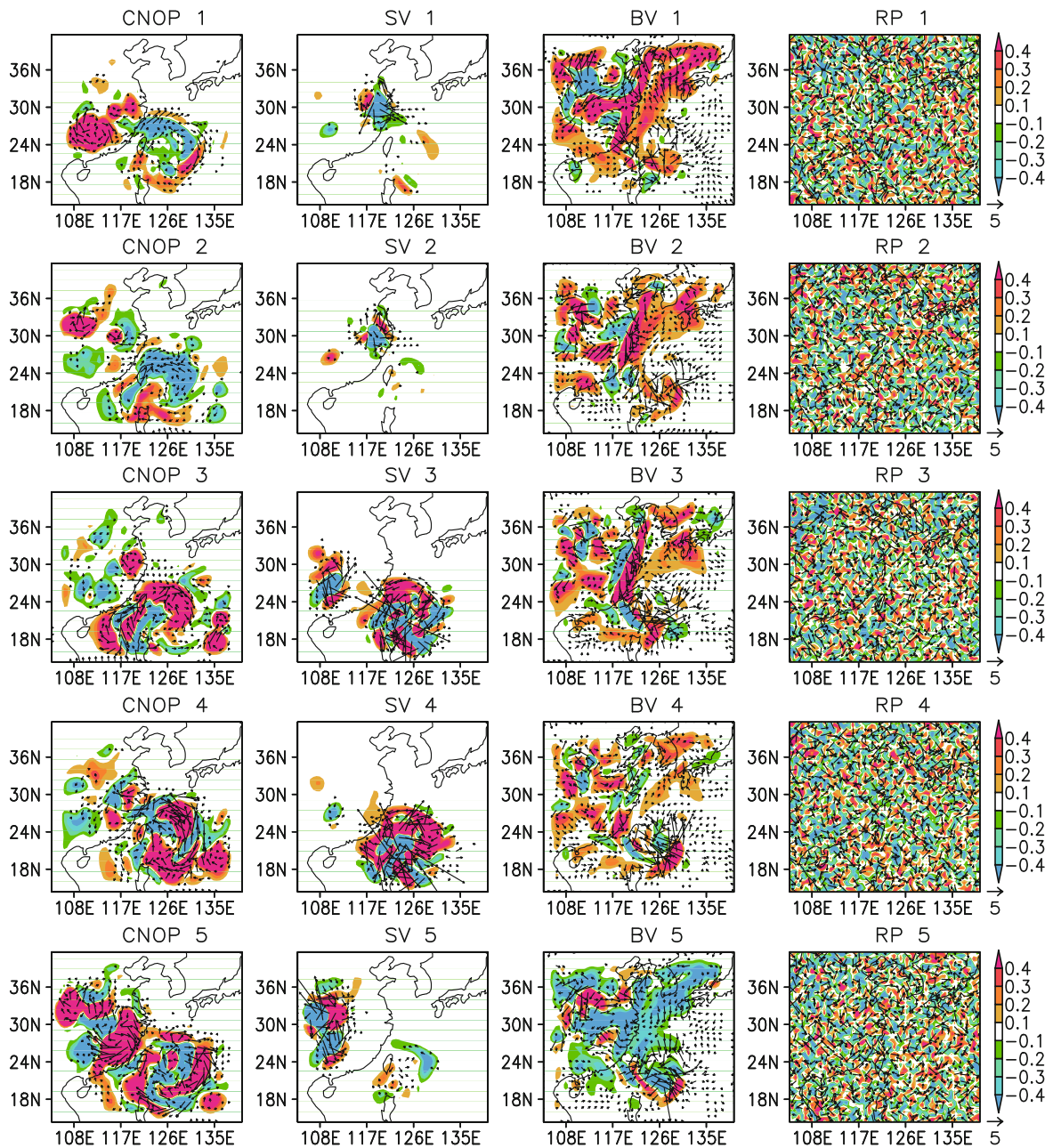


Fig. 2. Spatial structures of the temperature (color-shaded) and wind components (vectors) of the first five CNOPs, SVs, BVs and RPs with $\beta = 0.3 \times 9 \text{ J kg}^{-1}$ for STY Matsa (2005) at the level $\sigma = 0.975$. The columns list them in sequence, from the first to the fifth, respectively.

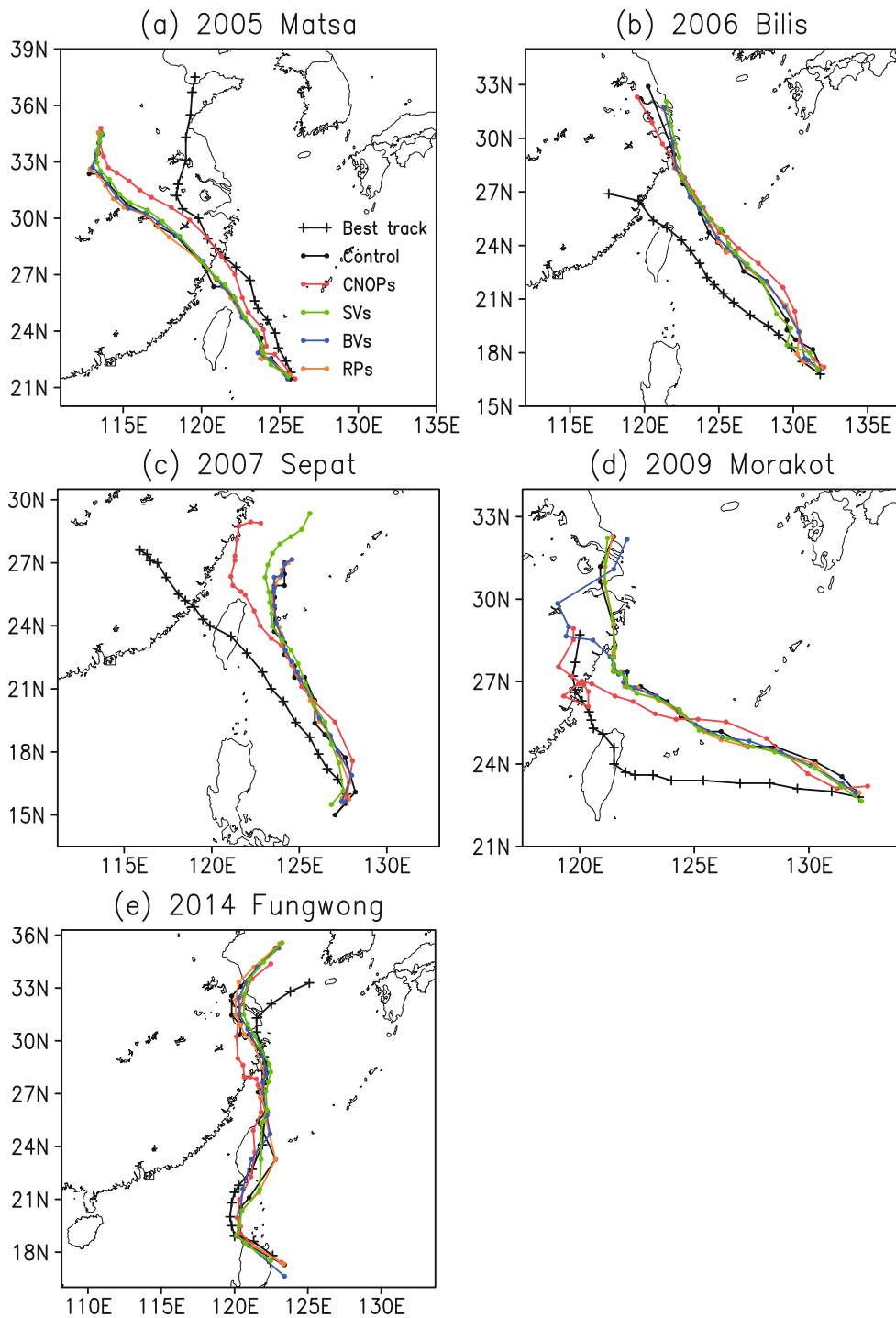


Fig. 3. Best tracks (black line with plus signs), tracks of the control forecast (black line with solid circles), and the orthogonal CNOPs– (red line with solid circles), SVs– (green line with solid circles), BVs– (blue line with solid circles), and RPs–based ensemble-mean forecasts (orange line with solid circles), with $\beta = 0.3 \times 9 \text{ J kg}^{-1}$, for the cases of (a) STY Matsa (2005), (b) STS Bilis (2006), (c) Super TY Septat (2007), (d) TY Morakot (2009), and (e) STS Fungwong (2014).

nal CNOPs–based ensemble-mean forecasts are much closer to the observed ones than those for the forecasts based on the other methods, especially for three TC cases: STY Matsa (2005), Super TY Septat (2007) and TY Morakot (2009). To

further demonstrate the superiority of orthogonal CNOPs–based ensemble-mean forecasts clearly, we show in Fig. 4a the averaged TC track forecast errors of all cases and all lead times of the forecasts (6 h, 12 h, . . . , 120 h), and in Fig. 4b the

corresponding improvements with respect to the control forecasts. It is clear that the forecast errors of the TC tracks are much smaller for the orthogonal CNOPs-based ensemble-mean forecasts than for those based on the other methods, and therefore the former improves the control forecast more than the latter. Figure 5a shows the TC track forecast errors of the control and ensemble-mean forecasts averaged for the five TC cases at lead times of 24 h, 48 h, 72 h, 96 h, and 120 h. The results show that the orthogonal CNOPs-based ensemble-mean forecasts do not improve the control forecasts at the lead time of 24 h (the reason can be seen in section 5.1); however, they improve the control forecasts and show higher skill than the orthogonal SVs-based ones at the lead time of 48 h. Particularly, at the 72-, 96- and 120-h lead times, the orthogonal CNOPs-based ensemble-

mean forecasts possess the smallest TC-track forecast errors among the ensemble forecasts based on the different methods and greatly improve the control forecasts. It is inferred that the orthogonal CNOPs-based ensemble forecast system, compared with the orthogonal SVs-, RPs- and BVs-based ensemble forecast systems, tends to possess the higher skill in forecasting the TC track, especially at longer lead times. Why, then, do the orthogonal CNOPs-based ensemble-mean forecasts possess higher forecast skill? Next, we attempt to uncover the possible reason.

It is known that the spread of the ensemble members (i.e., the ensemble spread) and the forecast error of the ensemble-mean forecast should be close for a good ensemble forecast system (Branković et al., 1990; Eckel and Mass, 2005; Buckingham et al., 2010), where the ensemble spread indicates

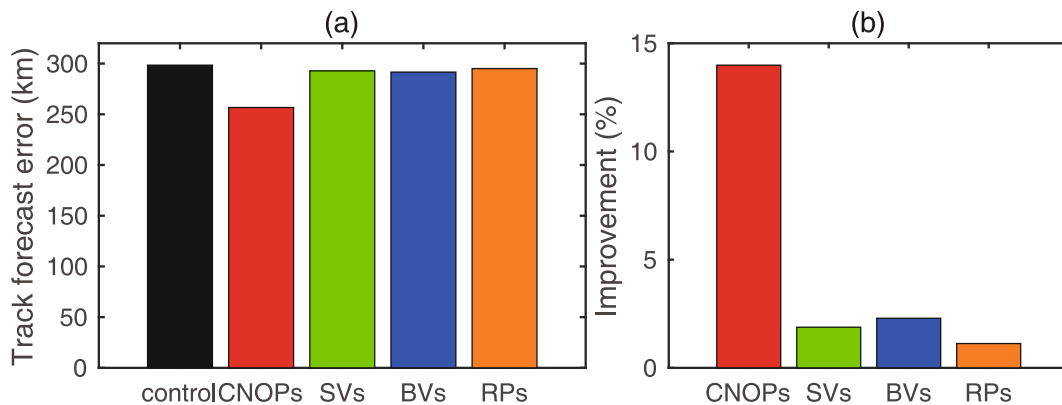


Fig. 4. (a) Averaged typhoon track forecast errors of the five typhoon cases and all the lead times of the forecasts (6 h, 12 h, . . . , 120 h), for the control forecast and the orthogonal CNOPs-, SVs-, BVs-, and RPs-based ensemble-mean forecasts, with $\beta = 0.3 \times 9 \text{ J kg}^{-1}$. (b) Improvement of the ensemble-mean forecast against the control forecast. The horizontal axis denotes the type of typhoon track, with the control (black) referring to the control forecast and CNOPs (red), SVs (green), BVs (blue) and RPs (orange), respectively, referring to the orthogonal CNOPs-, SVs-, BVs-, and RPs-based ensemble-mean forecasts. With the TC track forecast errors of all cases and all lead times of the forecasts (6 h, 12 h, . . . , 120 h) as samples, a paired *t*-test is performed, indicating that the improvement of the orthogonal CNOPs-based ensemble-mean forecast against those of the other methods is statistically significant at the 99% confidence level.

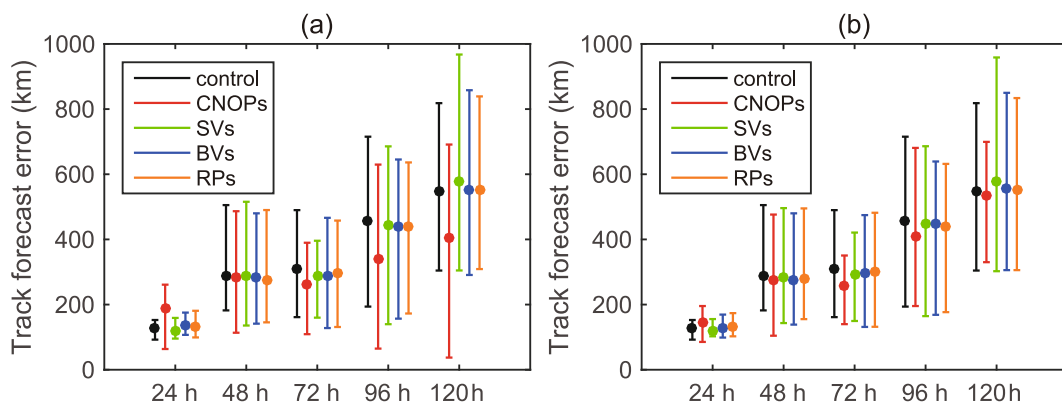


Fig. 5. Typhoon track forecast errors of the control forecast and the orthogonal CNOPs-, SVs-, BVs-, and RPs-based ensemble-mean forecasts for the five typhoon cases, where the lead times are 24 h, 48 h, 72 h, 96 h, and 120 h, and the magnitudes of the initial perturbations are (a) $\beta = 0.3 \times 9 \text{ J kg}^{-1}$ and (b) $\beta = 0.3 \times 4 \text{ J kg}^{-1}$. The dots denote the mean of the typhoon track forecast errors for all the typhoon cases; the error bars around each mean represent the maximum and minimum track forecast errors for the five typhoon cases.

the uncertainties of the ensemble forecast members (for the calculation, refer to the Appendix). However, most ensemble forecasting systems have the shortcoming of overly small ensemble spreads and present much larger gaps between their ensemble spreads and ensemble-mean forecast errors (Stensrud et al., 2000; Buckingham et al., 2010). The present study has shown that the orthogonal CNOPs-based ensemble-mean forecasts tend to possess higher forecast skills for TC tracks than those based on the other methods (see Fig. 5). However, does the ensemble forecast generated by the orthogonal CNOPs exhibit the smallest gap between its ensemble spread and ensemble-mean forecast error? To clarify this, in Fig. 6 we plot the average of the ensemble spreads for the five TC track forecasts and the averages of the ensemble-mean track forecast errors. It can be seen that the ensemble spreads of the orthogonal CNOPs-based ensemble forecasts are much larger than those of the orthogonal SVs-, BVs- and RPs-based ensemble forecasts; furthermore, the corresponding differences between the ensemble spreads and the ensemble-mean forecast errors are the smallest for the orthogonal CNOPs-based ensemble forecast system. The orthogonal CNOPs represent the optimal initial perturbations in the nonlinear model, which have the largest developments in their respective subspaces. As compared with orthogonal SVs, orthogonal CNOPs consider the effects of nonlinearities, which is essential for the nonlinear forecasts, especially in the forecast period after two days. So, it is conceivable that the ensemble forecast members generated by the orthogonal CNOPs possess much larger ensemble spreads. Furthermore, such a spread is shown to be closer to the ensemble-mean forecast error, which indicates that the orthogonal CNOPs-based ensemble forecast system provides a large but appropriate ensemble spread and overcomes the shortcoming of the smaller spreads that most ensemble forecasting systems

exhibit for the forecast members. This may be one of the reasons why the orthogonal CNOPs-based ensemble forecasts have the highest forecast skills for the TC tracks.

In addition, we have investigated the spatial distributions of the ensemble members generated by the different methods (Fig. 7). The results show that the ensemble forecast members generated by the orthogonal CNOPs tend to be located on the two sides of the observed TC track, while those generated by the other methods are more concentrated and leave the observed TC track at the edges or outside of the ensemble members. Obviously, the orthogonal CNOPs-based ensemble forecast members often include the observed TC track and are more useful for creating the ensemble-mean forecasts to capture the observed TC track and possess the highest skill.

5. Discussion

5.1. Reason for the lower forecast skills of the orthogonal CNOPs-based ensemble-mean forecasts at the lead time of 24 h

As stated in section 4, the orthogonal CNOPs-based ensemble-mean forecasts present lower forecast skills at the lead time of 24 h. In this section, we analyze the reason.

The orthogonal CNOPs represent the initial perturbations that have the largest growth in their respective phase subspaces at the final point of the optimization time period (i.e., 24 h). Therefore, at the final point of the optimization period, the ensemble members generated by the orthogonal CNOPs should have the largest ensemble spreads. Indeed, we find that the ensemble members generated by the orthogonal CNOPs show ensemble spreads with maximum uncertainties that can reach 274.88 km, while the averaged track forecast errors of the control forecasts of the five TC cases at 24 h is only 125.54 km (see Fig. 6). It is obvious that the spread of the ensemble members generated by the orthogonal CNOPs at a lead time of 24 h overestimates the uncertainties of the control forecast, which causes the ensemble-mean forecasts at the lead time of 24 h to present forecast errors even larger than those of the control forecasts.

But why do the ensemble members possess large spreads and overestimate the uncertainties of the control forecast at the lead time of 24 h? To address this question, we investigate the effects of the magnitude of the initial perturbations on the forecast skills of the ensemble-mean forecasts at the lead time of 24 h. Here, we choose the constraint conditions $\mathbf{x}_0^T \mathbf{C}_1 \mathbf{x}_0 \leq \beta$ with $\beta = 0.3 \times 4 \text{ J kg}^{-1}$ and $\beta = 0.3 \times 9 \text{ J kg}^{-1}$ to compute the orthogonal CNOPs for the optimization time of 24 h. Then, we compare the forecast skills of the orthogonal CNOPs-based ensemble-mean forecasts for these two constraint conditions. Figure 5b plots the ensemble-mean forecast error of the TC track when using $\beta = 0.3 \times 4 \text{ J kg}^{-1}$ to constrain the initial perturbations for the ensemble forecasts based on the different methods. It is shown that the orthogonal CNOPs-based ensemble-mean forecast still tends to show much higher forecast skills than those of the other methods at longer lead times. However, when comparing the results be-

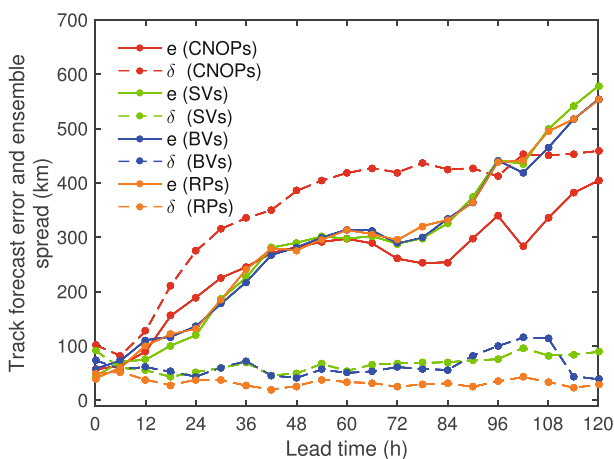


Fig. 6. Time-dependent spread (dashed lines) of the ensemble forecast members and the time-dependent forecast errors (solid lines) of the ensemble-mean forecasts, where both the spread and forecast error are estimated by calculating the means of the five typhoon cases with $\beta = 0.3 \times 9 \text{ J kg}^{-1}$. The relevant ensemble forecast methods are the same as in Fig. 4 and are denoted by the same colors as in Fig. 4.

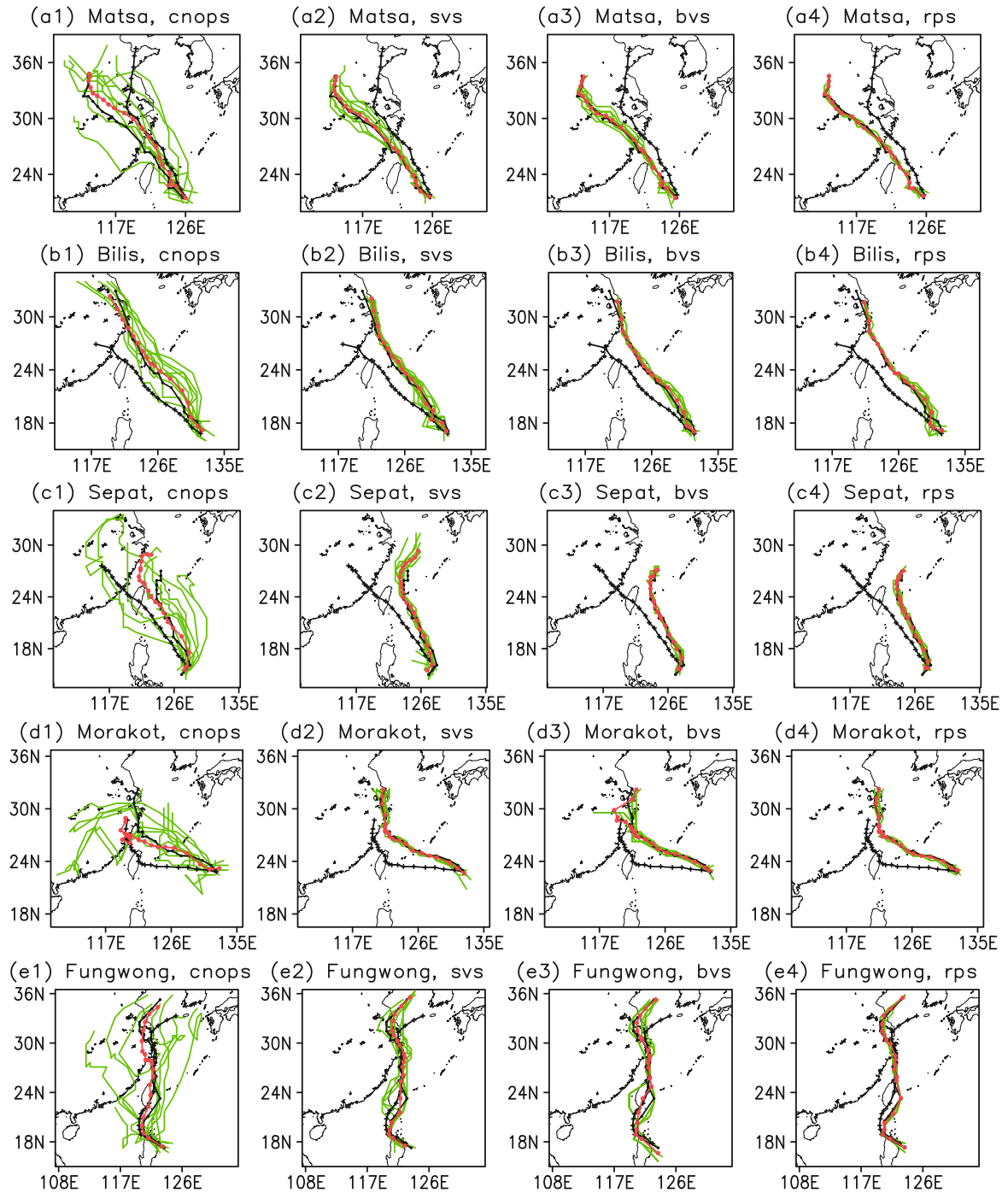


Fig. 7. Distributions of the typhoon best track (black line with plus signs) and the tracks of the control forecast (black line with solid circles), ensemble-mean forecast (red line with solid circles), and perturbed forecasts (green lines). The numbers 1–4 at the top of the subfigures represent the orthogonal CNOPs-, SVs-, BVs-, and RPs-based ensemble forecast techniques, with $\beta = 0.3 \times 9 \text{ J kg}^{-1}$, and the letters a, b, c, d and e denote the typhoon cases of STY Matsa (2005), STS Bilis (2006), Super TY Sepat (2007), TY Morakot (2009) and STS Fungwong (2014), respectively.

tween $\beta = 0.3 \times 4 \text{ J kg}^{-1}$ and $\beta = 0.3 \times 9 \text{ J kg}^{-1}$, we find that the former shows smaller forecast errors at the lead time of 24 h, increasing the forecast skill of the ensemble-mean forecast for the TC track with $\beta = 0.3 \times 9 \text{ J kg}^{-1}$ during the early period, but decreasing it during the later period. This shows that it is the large magnitude of orthogonal CNOPs that plays

negative roles in improving the forecast skill of the ensemble-mean forecast during the earlier periods of the forecast, which may interpret why the orthogonal CNOPs-based ensemble-mean forecasts show lower forecast skills at the lead time of 24 h. It is therefore inferred that the forecast skills of the orthogonal CNOPs-based ensemble-mean forecasts are re-

lated to the magnitude of the initial perturbations. Combining the results for $\beta = 0.3 \times 4 \text{ J kg}^{-1}$ and $\beta = 0.3 \times 9 \text{ J kg}^{-1}$, we would suggest that the orthogonal CNOPs-based ensemble-mean forecasts use small CNOP initial perturbations to generate the ensemble members for short-period forecasts, such as for less than three days; otherwise, they should adopt much larger CNOP initial perturbations. The exact magnitude of the CNOPs for ensemble forecasts remains to be explored in depth by future studies.

5.2. Forecast skills of the orthogonal CNOPs-based ensemble-mean forecasts for different TC cases

The above results are derived by evaluating the average forecast error of the five TC cases, and demonstrate that the orthogonal CNOPs are more favorable than the orthogonal SVs, RPs, and BVs for improving the ensemble forecast skills. Next, we investigate the forecast skills of the orthogonal CNOPs-based ensemble-mean forecasts for different TC cases. Figure 8 illustrates the evolution of the TC track forecast errors of the control forecasts and the ensemble-mean forecasts for each TC case, and Fig. 9a shows the means of the corresponding forecast errors of all the lead times (6 h, 12 h, . . . , 120 h) for each TC case. Specifically, for STY Matsa (2005), Super TY Sepat (2007) and TY Morakot (2009), the orthogonal CNOPs-based ensemble-mean forecasts improve their control forecast, and the improvement is much larger

than those of the orthogonal SVs-, RPs-, and BVs-based ensemble-mean forecasts. For STS Fungwong (2014), although the orthogonal CNOPs-based ensemble-mean forecast has a skill slightly lower than that of the orthogonal BVs-based ensemble-mean forecast, the skill is higher than those of the orthogonal SVs- and RPs-based ensemble-mean forecasts. However, for STS Bilis (2006), all the orthogonal CNOPs-, SVs-, RPs-, and BVs-based ensemble-mean forecasts fail to improve the control forecast skill, and the orthogonal CNOPs-based ensemble-mean forecast has the lowest skill. Why, then, does the orthogonal CNOPs-based ensemble-mean forecast show the lowest skill for STS Bilis (2006)?

One possible reason is related with the magnitude of the initial perturbations. Figure 9b shows the results of the experiment with $\beta = 0.3 \times 4 \text{ J kg}^{-1}$. It is shown that the track error of the orthogonal CNOPs-based ensemble-mean forecast for STS Bilis (2006) is largely reduced when the magnitude of the initial perturbations is reduced to $\beta = 0.3 \times 4 \text{ J kg}^{-1}$. Therefore, this result can be seen as evidence of the statement that the poor performance of the orthogonal CNOPs-based ensemble-mean forecast for STS Bilis (2006) is possibly due to the overly large initial perturbations. In fact, for a given reference state, the difference between the nonlinear evolution and the linear evolution of the initial perturbation increases with the magnitude of the initial perturbation, i.e.,

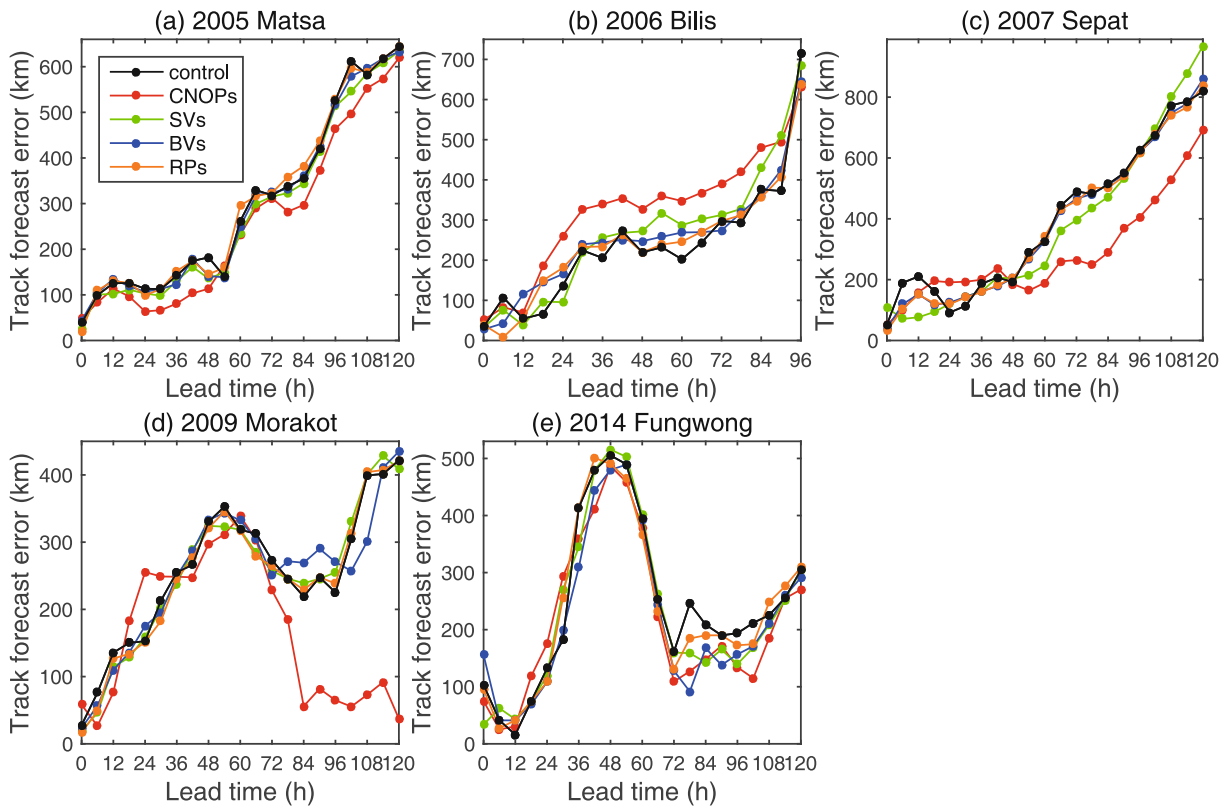


Fig. 8. Time-dependent forecast errors of the typhoon tracks for the control forecast (black line) and the orthogonal CNOPs (red line)-, SVs (green line)-, BVs (blue line)-, and RPs (orange line)-based ensemble-mean forecasts, with $\beta = 0.3 \times 9 \text{ J kg}^{-1}$, for the typhoon cases of (a) STY Matsa (2005), (b) STS Bilis (2006), (c) Super TY Sepat (2007), (d) TY Morakot (2009), and (e) STS Fungwong (2014).

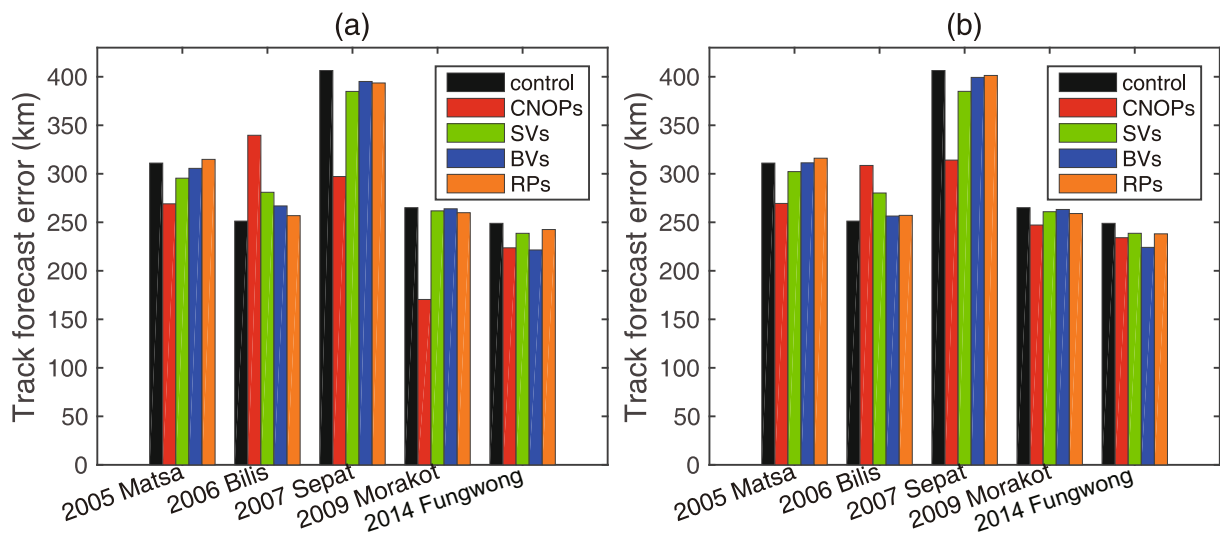


Fig. 9. Mean forecast errors of the control forecast (black) and the orthogonal CNOPs–based (red), SVs–based (green), BVs–based (blue), and RPs–based (orange) ensemble-mean forecasts for the five typhoon cases and all lead times (6 h, 12 h, . . . , 120 h), and initial-perturbation magnitudes of (a) $\beta = 0.3 \times 9 \text{ J kg}^{-1}$ and (b) $\beta = 0.3 \times 4 \text{ J kg}^{-1}$.

the initial perturbations of large magnitude evolve more nonlinearly than those of small magnitude. In the present study, for all the TC cases, the orthogonal CNOPs are calculated with the same magnitude. Therefore, the orthogonal CNOPs for STS Bilis (2006) could be too large and then overestimate the nonlinearities existing in the control forecasts. Note that the orthogonal CNOPs represent the fastest growing initial perturbations in their relevant subspaces and have much larger perturbation growths than those of the BVs and SVs. This encourages BVs and SVs to show much weaker nonlinear behaviors and be more likely to depict the nonlinear behavior of STS Bilis (2006), and to show higher skill in the ensemble-mean forecast for STS Bilis (2006) than the orthogonal CNOPs–based ensemble-mean forecasts. In addition, we notice that for STS Bilis (2006), when the magnitude of the initial perturbations is reduced to $\beta = 0.3 \times 4 \text{ J kg}^{-1}$, the track errors of the orthogonal SVs– and RPs–based ensemble-mean forecasts change negligibly, but the track errors of the BVs– and CNOPs–based ensemble-mean forecasts are obviously reduced, with the latter reduction being more significant. This indicates that the sensitivity of ensemble forecasts (especially the CNOPs–based ensemble forecasts) to initial perturbation magnitudes also influences its skill. Therefore, an appropriate magnitude of initial perturbations helps achieve a much higher forecast skill for ensemble forecasts, which also sheds light on why the CNOPs–based ensemble forecasts show much lower forecast skill for STS Bilis (2006).

Another possible reason is related with the model errors. We compare the values of the cost functions [as shown in Eq. (1)] corresponding to the first five CNOPs for the different TC cases (see Table 2). It is found that the values of the cost function of the CNOPs for STS Bilis (2006) are the smallest of those for the considered TC cases, despite the CNOPs having the same amplitude for different TC cases. This in-

dicates that STS Bilis (2006) is the least sensitive to initial perturbations among our investigated TC cases. This implies that the forecast for STS Bilis (2006), compared with those of other TC cases, is greatly influenced by model errors. Despite the ensemble forecast members generated by the RPs, BVs, and SVs, compared with those generated by the orthogonal CNOPs, estimating more appropriately the nonlinear growth of the initial analysis errors, they cannot capture the effect of the model errors on the forecast for STS Bilis (2006). All these aspects may explain why all the above ensemble-mean forecasts fail to show high forecast skill for STS Bilis (2006). It is therefore inferred that the skill of the ensemble forecasts for STS Bilis (2006) may be greatly improved by considering ensemble forecasts associated with model errors.

5.3. Ensemble forecast skill for TC intensity

In addition to the TC-track forecast, we also analyze the skills of the ensemble forecasts for TC intensity based on the different methods. Figure 10 illustrates the evolution of the minimum sea level pressure of the control forecasts and the ensemble-mean forecasts for each TC case. The results show that the TC intensities simulated by MM5 are often significantly underestimated when they are strong but overestimated when they are weak. This may be due to the model horizontal resolution in this work not being fine enough to describe the TC structure and intensity realistically, and MM5 has model errors such as inaccurate descriptions of physical processes.

Notably, there are huge gaps between the observed and modeled initial intensity of STS Bilis (2006), Super TY Sepat (2007), and STS Fungwong (2014) in Fig. 10. In the present study, we use NCEP FNL data to generate the initial conditions. It has been revealed previously that these data possess large differences with observations of TC intensity for TC cases (Zhou et al., 2016). Thus, when using the FNL data to generate the initial conditions, the modeled initial intensity of

Table 2. The values of the cost function [as in the Eq. (1)] corresponding to the first five CNOPs for the five typhoon cases.

CNOP	Case				
	2005 STY Matsa	2006 STS Bilis	2007 Super TY Sepat	2009 TY Morakot	2014 STS Fungwong
1	279.09	81.69	119.76	104.40	116.42
2	221.25	72.42	99.61	97.80	93.02
3	195.97	70.69	96.67	83.94	82.20
4	149.64	63.37	90.47	82.39	80.75
5	149.62	63.10	81.96	77.82	72.74

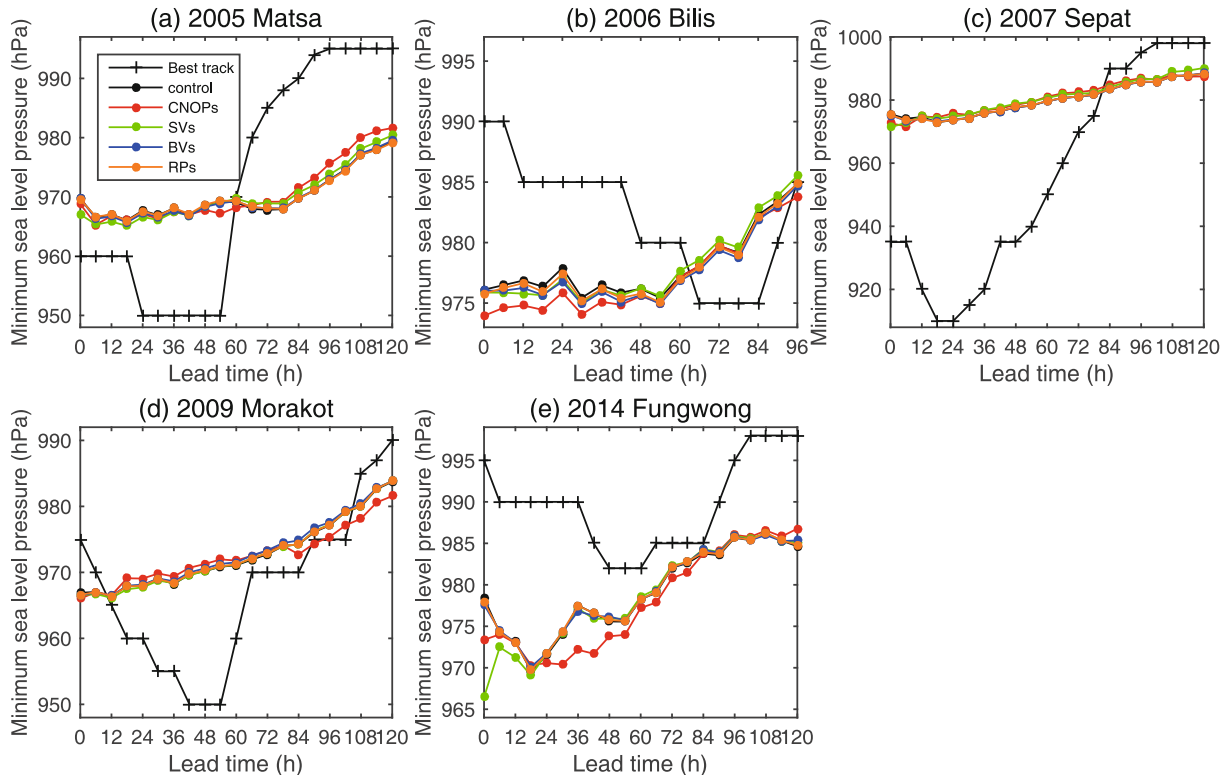


Fig. 10. Time-dependent minimum sea level pressure for the observation (black line with plus signs), control forecast (black line with solid circles), and the orthogonal CNOPs (red line with solid circles)–, SVs (green line with solid circles)–, BVs (blue line with solid circles)–, and RPs (orange line with solid circles)–based ensemble-mean forecasts, with $\beta = 0.3 \times 9 \text{ J kg}^{-1}$, for the typhoon cases of (a) STY Matsa (2005), (b) STS Bilis (2006), (c) Super TY Sepat (2007), (d) TY Morakot (2009), and (e) STS Fungwong (2014).

the TCs will have obvious bias compared with observations. That is, the huge gaps between the observed and modeled initial intensity in the present study may be caused by the FNL data. Zhou et al. (2016) showed that when the initial TC intensity error is sizeable, the TC-track forecast skill can be greatly increased by improving the geopotential height and wind fields in and around the TC center at the initial time (i.e., improving the model initial intensity of TCs). Therefore, we infer that the TC-track forecasts in the present study can be further improved if the initial intensity is better described by the model. However, MM5, together with FNL data, cannot estimate the TC intensities well. It is therefore expected that future work can improve the forecast skill of the TC intensity forecast and then further increase the skill of the TC-track forecasts.

As discussed above, the model horizontal resolution in

this work is not suitable to discuss TC intensity. The results show that all the methods, including the orthogonal CNOPs–based method cannot effectively improve the forecast skill of TC intensity. In other words, the ensemble forecasts with only the initial perturbations in this work do not increase the forecast skill of TC intensity. This may be related to both the coarse model horizontal resolution used in this work and the model error. In fact, previous studies (Zhao et al., 2007; Zhao and Wang, 2008) have also shown that large differences exist between the sea level pressures forecasted by MM5 and those observed, indicating the role of model errors in forecasting the TC intensity. In addition, as TCs originate and absorb energy from the ocean and stay over the ocean during most of their lifetime, the ocean will influence the development of TCs considerably. Therefore, ocean–typhoon feedbacks are essential to the forecasting of TCs. However, MM5 does not

sufficiently consider the effects of ocean–typhoon feedbacks and involves model errors. These model errors encourage us to consider the ensemble forecasts with multiple models or model perturbations. For the latter, the nonlinear forcing singular vectors (NFSVs) method has been proposed by Duan and Zhou (2013). NFSVs describe the model tendency errors that have the largest impact on the forecast results in nonlinear models (Duan and Zhou, 2013; Duan and Zhao, 2015). Therefore, when the model horizontal resolution is increased to be suitable for the simulation of TC intensity, model perturbations with NFSVs may improve the forecasting of TC intensity, and it is expected that ensemble forecasts with both orthogonal CNOPs and NFSVs can increase the ensemble forecast skill of not only TC track but also TC intensity.

6. Summary

Following the simple Lorenz-96 model in Duan and Huo (2016), the present study further applies orthogonal CNOPs in a much more realistic model, MM5, for the ensemble forecasting of TC tracks. As shown in the comparisons among the orthogonal CNOPs and SVs, BVs, and RPs, the orthogonal CNOPs–based ensemble forecasting technique possesses the highest skill in forecasting the TC track. By identifying the reasons for this, the results of this work show that the orthogonal CNOPs–based ensemble forecasting technique, compared with those based on other methods, exhibits an ensemble spread that is much larger but often includes the real TC track within the members. This makes it more likely for the resultant ensemble spread of the orthogonal CNOPs to be closer to the ensemble-mean forecast error, and makes the orthogonal CNOPs–based ensemble forecasts show much higher forecast skills.

The results show that the lower forecast skills of the orthogonal CNOPs–based ensemble-mean forecasts at 24 h are related to the overly large initial perturbations. In addition, the present study also demonstrates that the decreased magnitudes of the initial perturbations may help increase the skill of the orthogonal CNOPs–based ensemble-mean forecasts in the early forecast period, but greatly reduce it in the latter period. This suggests that orthogonal CNOPs of small magnitude are useful for yielding ensemble-mean forecasts with higher skill for short-period forecasts; on the contrary, those of large magnitude are feasible for much longer-period forecasts. It is therefore inferred that, if one wants to achieve an ensemble-mean forecast with acceptable skill during both the early and later periods, orthogonal CNOPs of different magnitude should be adopted to derive the initial ensemble perturbations. Thus, more experiments should be conducted in the future to reveal a rule to determine the magnitude of the orthogonal CNOPs in the ensemble forecasts. In addition, the optimization time to yield the orthogonal CNOPs may also influence the skill of the ensemble forecasts. Therefore, more studies are also needed to explore whether there exists an optimal combination of initial perturbation magnitudes and optimization times to achieve the highest skill for the ensemble forecasts.

The present study also discusses the forecasting of TC intensity. Unfortunately, all of the abovementioned ensemble forecast techniques cannot improve these results effectively, and even reduce the forecast skill of the TC intensity. Since these ensemble forecast techniques are related to perturbing the initial conditions, the reduced ensemble forecast skill for TC intensity may indicate that the forecasting of TC intensity may be related to both the coarse model horizontal resolution and the model error. As such, model perturbations such as those described by the tendency perturbations of the NFSV structures could be necessary to improve forecasts of TC intensity when the model horizontal resolution is increased to be suitable for the simulation of TC intensity. The forecast may be influenced by not only the initial errors, but also model errors. Therefore, in ensemble forecasts, one should perturb both the initial conditions and the model itself to estimate the uncertainties induced by the initial errors and model errors, ultimately achieving a much higher forecast skill. Tracton et al. (1998) and Hou et al. (2001) also showed similar perspectives and proposed that ensemble forecasts with only initial perturbations, rather than those with both initial perturbations and multimodel or multiphysical parameterization schemes or model perturbations, show much lower forecast skill. Thus, it is expected that ensemble forecasts with both orthogonal CNOPs and NFSVs can be used to increase the ensemble forecast skill of not only the TC track, but also the TC intensity, when the model horizontal resolution is increased to be suitable for the simulation of TC intensity.

The above results are derived from five TC cases and are only indicative. The orthogonal CNOPs method is new and the related computation is presently time-consuming. A highly efficient solver is therefore expected to be developed, and then more TC cases can be adopted to investigate the orthogonal CNOPs–based ensemble forecast technique and validate the results in the present study. Operational suggestions can then be provided. In addition, the objective function used to calculate the orthogonal CNOPs is the dry energy of the perturbation at the end of the optimization period, which cannot directly reflect the forecast of the TC track and intensity. So, what about an objective function that is defined as the moist energy of the perturbation or the forecast error of the TC intensity? Only 11 ensemble members are used in the present study. Thus, what about the ensemble forecast skill for more ensemble members? The above questions are all worthy of future investigation.

Acknowledgements. This work was jointly sponsored by the National Key Research and Development Program of China (2018YFC1506402), the National Natural Science Foundation of China (Grant Nos. 41475100 and 41805081), and the Global Regional Assimilation and Prediction System Development Program of the China Meteorological Administration (GRAPES-FZZX-2018). The FNL data used in this study can be obtained from <http://rda.ucar.edu/datasets/ds083.2/>. The historical TC data are available at http://tcdata.typhoon.org.cn/en/zjljsjj_zlhq.html.

APPENDIX

Forecast errors of TC track

The TC tracks are identified by the TC center locations, which are identified by the locations where the sea level pressures are minimal. The forecast error of the TC track is that of the TC center locations, which is determined by the great-circle distance between the two points on the Earth. Assume that $F = (a_f, y_f)$ is the central location of the forecast TC and $A = (a_o, y_o)$ is that of the observed TC, where a_f and a_o are the longitudes and y_f and y_o are the latitudes. Then, the forecast error of the TC track at some forecast time can be expressed as

$$|F - A| = 111.11 \cos^{-1} [\sin y_o \sin y_f + \cos y_o \cos y_f \cos(a_o - a_f)]. \quad (A1)$$

Ensemble spread

The ensemble spread is the RMSE of the ensemble forecast members with respect to the ensemble mean, i.e., $\delta = \sqrt{\frac{1}{N} \sum_{i=1}^N |F_i - \bar{F}|^2}$, where $\bar{F} = \frac{1}{N} \sum_{i=1}^N F_i$ is the ensemble mean, and $|F_i - \bar{F}|$ is the great-circle distance between ensemble member F_i and ensemble-mean \bar{F} . A good ensemble forecast system should have a suitable ensemble spread. If the ensemble spread is too small, one cannot effectively estimate the forecast uncertainty and it causes the true state to be located outside of the forecast ensemble, in turn causing a low forecast skill for the true state. If the ensemble spread is too large, additional errors are easily introduced, thus bringing about negative influences on the forecast results.

Improvement

Improvement of the ensemble-mean forecast over the control forecast is described by s :

$$s = \frac{E_c - E_e}{E_c} \times 100\%, \quad (A2)$$

where E_c is the forecast error of the control forecast and E_e is the forecast error of the ensemble-mean forecast. The ensemble-mean forecast improves the skill of the control forecast when $s > 0$. Otherwise, the ensemble-mean forecast does not increase the skill of the control forecast. The larger the value of s , the higher the skill of the ensemble-mean forecast.

REFERENCES

Anderson, J. L., 1997: The impact of dynamical constraints on the selection of initial conditions for ensemble predictions: Low-order perfect model results. *Mon. Wea. Rev.*, **125**(11), 2969–2983, [https://doi.org/10.1175/1520-0493\(1997\)125<2969:TIODCO>2.0.CO;2](https://doi.org/10.1175/1520-0493(1997)125<2969:TIODCO>2.0.CO;2).

Birgin, E. G., J. M. Martinez, and M. Raydan, 2000: Nonmonotone spectral projected gradient methods on convex sets. *SIAM Journal on Optimization*, **10**, 1196–1211, <https://doi.org/10.1137/S1052623497330963>.

Branković, Č., T. N. Palmer, F. Molteni, S. Tibaldi, and U. Cubasch, 1990: Extended-range predictions with ECMWF models: Time-lagged ensemble forecasting. *Quart. J. Roy. Meteor. Soc.*, **116**, 867–912, <https://doi.org/10.1002/qj.49711649405>.

Buckingham, C., T. Marchok, I. Ginis, L. Rothstein, and D. Rowe, 2010: Short- and medium-range prediction of tropical and transitioning cyclone tracks within the NCEP global ensemble forecasting system. *Wea. Forecasting*, **25**(6), 1736–1754, <https://doi.org/10.1175/2010WAF2222398.1>.

Buizza, R., P. L. Houtekamer, G. Pellerin, Z. Toth, Y. Zhu, and M. Wei, 2005: A comparison of the ECMWF, MSC, and NCEP global ensemble prediction systems. *Mon. Wea. Rev.*, **133**, 1076–1097, <https://doi.org/10.1175/MWR2905.1>.

Cheung, K. K. W., 2001: Ensemble forecasting of tropical cyclone motion: Comparison between regional bred modes and random perturbations. *Meteor. Atmos. Phys.*, **78**, 23–34, <https://doi.org/10.1007/s007030170003>.

Chien, F. C., and B. J. D. Jou, 2004: MM5 ensemble mean precipitation forecasts in the Taiwan area for three early summer convective (Mei-Yu) seasons. *Wea. Forecasting*, **19**, 735–750, [https://doi.org/10.1175/1520-0434\(2004\)019<0735:MEMPFI>2.0.CO;2](https://doi.org/10.1175/1520-0434(2004)019<0735:MEMPFI>2.0.CO;2).

Duan, W. S., and M. Mu, 2009: Conditional nonlinear optimal perturbation: Applications to stability, sensitivity, and predictability. *Science in China Series D: Earth Sciences*, **52**(7), 883–906, <https://doi.org/10.1007/s11430-009-0090-3>.

Duan, W. S., and F. F. Zhou, 2013: Non-linear forcing singular vector of a two-dimensional quasi-geostrophic model. *Tellus A*, **65**, 18452, <https://doi.org/10.3402/tellusa.v65i0.18452>.

Duan, W. S., and P. Zhao, 2015: Revealing the most disturbing tendency error of Zebiak–Cane model associated with El Niño predictions by nonlinear forcing singular vector approach. *Climate Dyn.*, **44**, 2351–2367, <https://doi.org/10.1007/s00382-014-2369-0>.

Duan, W. S., and Z. H. Huo, 2016: An approach to generating mutually independent initial perturbations for ensemble forecasts: orthogonal conditional nonlinear optimal perturbations. *J. Atmos. Sci.*, **73**, 997–1014, <https://doi.org/10.1175/JAS-D-15-0138.1>.

Duan, W. S., M. Mu, and B. Wang, 2004: Conditional nonlinear optimal perturbations as the optimal precursors for El Niño–Southern Oscillation events. *J. Geophys. Res.*, **109**, D23105, <https://doi.org/10.1029/2004JD004756>.

Dudhia, J., 1993: A nonhydrostatic version of the Penn state–NCAR mesoscale model: Validation tests and simulation of an Atlantic cyclone and cold front. *Mon. Wea. Rev.*, **121**, 1493–1513, [https://doi.org/10.1175/1520-0493\(1993\)121<1493:ANVOTP>2.0.CO;2](https://doi.org/10.1175/1520-0493(1993)121<1493:ANVOTP>2.0.CO;2).

Eckel, F. A., and C. F. Mass, 2005: Aspects of effective mesoscale, short-range ensemble forecasting. *Wea. Forecasting*, **20**(3), 328–350, <https://doi.org/10.1175/WAF843.1>.

Eom, H. S., and S. Myoung-Seok, 2011: Seasonal and diurnal variations of stability indices and environmental parameters using NCEP FNL data over East Asia. *Asia-Pacific Journal of Atmospheric Sciences*, **47**(2), 181–192, <https://doi.org/10.1007/s13143-011-0007-x>.

General Administration of Quality Supervision, Inspection and

- Quarantine of the People's Republic of China, Standardization Administration of the People's Republic of China, 2006: GB/T 19201—2006 Grade of tropical cyclones. Standards Press of China, Beijing [Available online at http://tcdata.typhoon.org.cn/doc/TC_std.pdf]. (in Chinese)
- Gilmour, I., and L. A. Smith, 1998: Enlightenment in shadows. *Nonlinear Dynamics and Stochastic Systems near the Millennium. AIP Conference Proceedings*, J. B. Kadtko and A. Bulsara, Eds., American Institute of Physics, 335–340.
- Grell, G. A., J. Dudhia, and D. R. Stauffer, 1994: A description of the fifth-generation Penn State/NCAR Mesoscale Model (MM5). NCAR Technical Note NCAR/TN-398+STR, 138pp, <https://doi.org/10.5065/D60Z716B>.
- Hou, D. C., E. Kalnay, and K. K. Droegemeier, 2001: Objective verification of the SAMEX'98 ensemble forecasts. *Mon. Wea. Rev.*, **129**, 73–91, [https://doi.org/10.1175/1520-0493\(2001\)129<0073:OVOTSE>2.0.CO;2](https://doi.org/10.1175/1520-0493(2001)129<0073:OVOTSE>2.0.CO;2).
- Hsiao, L. F., M. S. Peng, D. S. Chen, K. N. Huang, and T. C. Yeh, 2009: Sensitivity of typhoon track predictions in a regional prediction system to initial and lateral boundary conditions. *Journal of Applied Meteorology and Climatology*, **48**(9), 1913–1928, <https://doi.org/10.1175/2009JAMC2038.1>.
- Hwang, S., W. Graham, J. L. Hernandez, C. Martinez, J. W. Jones, and A. Adams, 2011: Quantitative spatiotemporal evaluation of dynamically downscaled mm5 precipitation predictions over the Tampa bay region, Florida. *Journal of Hydrometeorology*, **12**, 1447–1464, <https://doi.org/10.1175/2011JHM1309.1>.
- Jiang, Z. N., and M. Mu, 2009: A comparison study of the methods of conditional nonlinear optimal perturbations and singular vectors in ensemble prediction. *Adv. Atmos. Sci.*, **26**, 465–470, <https://doi.org/10.1007/s00376-009-0465-6>.
- Jiang, Z. N., and D. H. Wang, 2012: Conditional nonlinear optimal perturbations: Behaviour during the evolution of cold vortices over northeast China. *Quart. J. Roy. Meteor. Soc.*, **138**, 198–208, <https://doi.org/10.1002/qj.913>.
- Langland, R. H., M. A. Shapiro, and R. Gelaro, 2002: Initial condition sensitivity and error growth in forecasts of the 25 January 2000 East Coast Snowstorm. *Mon. Wea. Rev.*, **130**, 957–974, [https://doi.org/10.1175/1520-0493\(2002\)130<0957:ICSAEG>2.0.CO;2](https://doi.org/10.1175/1520-0493(2002)130<0957:ICSAEG>2.0.CO;2).
- Leith, C. E., 1974: Theoretical skill of monte Carlo forecasts. *Mon. Wea. Rev.*, **38**, 97–110, [https://doi.org/10.1175/1520-0493\(1974\)102<0409:TSOMCF>2.0.CO;2](https://doi.org/10.1175/1520-0493(1974)102<0409:TSOMCF>2.0.CO;2).
- Leutbecher, M., and T. N. Palmer, 2008: Ensemble forecasting. *J. Comput. Phys.*, **227**, 3515–3539, <https://doi.org/10.1016/j.jcp.2007.02.014>.
- Li, H. L., J. X. Peng, and Y. X. Zhang, 2014: Analysis on the role of various observation data in LAPS mesoscale analysis fields. *Torrential Rain and Disasters*, **33**(3), 273–280, <https://doi.org/10.3969/j.issn.1004-9045.2014.03.010>. (in Chinese)
- Liang, X. D., B. Wang, J. C. Chan, Y. H. Duan, D. L. Wang, Z. H. Zeng, and M. Leiming, 2007: Tropical cyclone forecasting with model-constrained 3D-Var. II: Improved cyclone track forecasting using AMSU-A, QuikSCAT and cloud-drift wind data. *Quart. J. Roy. Meteor. Soc.*, **133**, 155–165, <https://doi.org/10.1002/qj.10>.
- Lorenz, E. N., 1963: Deterministic nonperiodic flow. *J. Atmos. Sci.*, **20**, 131–141, [https://doi.org/10.1175/1520-0469\(1963\)020<0130:DNF>2.0.CO;2](https://doi.org/10.1175/1520-0469(1963)020<0130:DNF>2.0.CO;2).
- Lorenz, E. N., 1965: A study of the predictability of a 28-variable atmospheric model. *Tellus*, **17**, 321–333, <https://doi.org/10.1111/j.2153-3490.1965.tb01424.x>.
- Lorenz, E. N., 1995: Predictability: A problem partly solved. *Proc. Workshop on Predictability*, Shinfield Park, Reading, ECMWF, 18pp.
- Molteni, F., R. Buizza, T. N. Palmer, and T. Petroliagis, 1996: The ECMWF ensemble prediction system: Methodology and validation. *Quart. J. Roy. Meteor. Soc.*, **122**, 73–119, <https://doi.org/10.1002/qj.49712252905>.
- Mu, M., and Z. Y. Zhang, 2006: Conditional nonlinear optimal perturbations of a two-dimensional Quasigeostrophic model. *J. Atmos. Sci.*, **63**, 1587–1604, <https://doi.org/10.1175/JAS3703.1>.
- Mu, M., and Z. N. Jiang, 2008: A new approach to the generation of initial perturbations for ensemble prediction: Conditional nonlinear optimal perturbation. *Chinese Science Bulletin*, **53**(13), 2062–2068, <https://doi.org/10.1007/s11434-008-0272-y>.
- Mu, M., W. S. Duan, and B. Wang, 2003: Conditional nonlinear optimal perturbation and its applications. *Nonlinear Processes in Geophysics*, **10**, 493–501, <https://doi.org/10.5194/npg-10-493-2003>.
- Mu, M., F. F. Zhou, and H. L. Wang, 2009: A method for identifying the sensitive areas in targeted observations for tropical cyclone prediction: Conditional nonlinear optimal perturbation. *Mon. Wea. Rev.*, **137**, 1623–1639, <https://doi.org/10.1175/2008MWR2640.1>.
- Mu, M., F. F. Zhou, X. H. Qin, and B. Y. Chen, 2014: The application of conditional nonlinear optimal perturbation to targeted observations for tropical cyclone prediction. *Frontiers in Differential Geometry, Partial Differential Equations and Mathematical Physics*, Ge et al., Eds, World Scientific, 291–325, https://doi.org/10.1142/9789814578097_0018.
- Mureau, R., F. Molteni, and T. N. Palmer, 1993: Ensemble prediction using dynamically conditioned perturbations. *Quart. J. Roy. Meteor. Soc.*, **119**, 299–323, <https://doi.org/10.1002/qj.49711951005>.
- Pessi, A. T., and S. Businger, 2009: The impact of lightning data assimilation on a winter storm simulation over the North Pacific Ocean. *Mon. Wea. Rev.*, **137**, 3177–3195, <https://doi.org/10.1175/2009MWR2765.1>.
- Pu, Z. X., E. Kalnay, D. Parrish, W. S. Wu, and Z. Toth, 1997: The use of bred vectors in the NCEP global 3D Variational analysis system. *Wea. Forecasting*, **12**, 689–695, [https://doi.org/10.1175/1520-0434\(1997\)012<0689:TUOBVI>2.0.CO;2](https://doi.org/10.1175/1520-0434(1997)012<0689:TUOBVI>2.0.CO;2).
- Qin, X. H., and M. Mu, 2011: A study on the reduction of forecast error variance by three adaptive observation approaches for tropical cyclone prediction. *Mon. Wea. Rev.*, **139**, 2218–2232, <https://doi.org/10.1175/2010MWR3327.1>.
- Qin, X. H., W. S. Duan, and M. Mu, 2013: Conditions under which CNOP sensitivity is valid for tropical cyclone adaptive observations. *Quart. J. Roy. Meteor. Soc.*, **139**, 1544–1554, <https://doi.org/10.1002/qj.2109>.
- Simon, H. D., 1984: The Lanczos algorithm with partial reorthogonalization. *Mathematics of Computation*, **165**(42), 115–142, <https://doi.org/10.2307/2007563>.
- Skamarock, W. C., J. B. Klemp, J. Dudhia, D. O. Gill, D. M. Barker, W. Wang, and J. G. Powers, 2005: A description of the advanced research WRF version 2. NCAR Technical Note NCAR/TN-468+STR, 88 pp.
- Stensrud, D. J., J. W. Bao, and T. T. Warner, 2000: Using initial condition and model physics perturbations in short-range ensemble simulations of mesoscale convective systems. *Mon.*

- Wea. Rev.*, **128**, 2077–2107, [https://doi.org/10.1175/1520-0493\(2000\)128<2077:UICAMP>2.0.CO;2](https://doi.org/10.1175/1520-0493(2000)128<2077:UICAMP>2.0.CO;2).
- Toth, Z., and E. Kalnay, 1993: Ensemble forecasting at NMC: the generation of perturbations. *Bull. Amer. Meteor. Soc.*, **74**, 2317–2330, [https://doi.org/10.1175/1520-0477\(1993\)074<2317:EFANTG>2.0.CO;2](https://doi.org/10.1175/1520-0477(1993)074<2317:EFANTG>2.0.CO;2).
- Toth, Z., and E. Kalnay, 1997: Ensemble forecasting at NCEP and the breeding method. *Mon. Wea. Rev.*, **125**, 3297–3319, [https://doi.org/10.1175/1520-0493\(1997\)125<3297:EFANAT>2.0.CO;2](https://doi.org/10.1175/1520-0493(1997)125<3297:EFANAT>2.0.CO;2).
- Tracton, M. S., J. Du, Z. Toth, and H. Juang, 1998: Short-range ensemble forecasting (SREF) at NCEP/EMC. *Preprints of 12th Conference on Numerical Weather Prediction*, Phoenix, AZ, Amer. Meteor. Soc., 269–272.
- Wei, C. C., 2012: Wavelet support vector machines for forecasting precipitation in tropical cyclones: Comparisons with GSVM, regression, and MM5. *Wea. Forecasting*, **27**, 438–450, <https://doi.org/10.1175/WAF-D-11-00004.1>.
- Yamaguchi, M., R. Sakai, M. Kyoda, T. Komori, and T. Kadowaki, 2009: Typhoon ensemble prediction system developed at the Japan meteorological agency. *Mon. Wea. Rev.*, **137**, 2592–2604, <https://doi.org/10.1175/2009MWR2697.1>.
- Yamaguchi, M., T. Nakazawa, and K. Aonashi, 2012: Tropical cyclone track forecasts using JMA model with ECMWF and JMA initial conditions. *Geophys. Res. Lett.*, **39**, L09801, <https://doi.org/10.1029/2012GL051473>.
- Yang, L., D. X. Wang, and S. Q. Peng, 2012: Comparison between MM5 simulations and satellite measurements during Typhoon Chanchu (2006) in the South China Sea. *Acta Oceanologica Sinica*, **31**(2), 33–44, <https://doi.org/10.1007/s13131-012-0190-3>.
- Ying, M., W. Zhang, H. Yu, X. Q. Lu, J. X. Feng, Y. X. Fan, Y. T. Zhu, and D. Q. Chen, 2014: An overview of the China meteorological administration tropical cyclone database. *J. Atmos. Oceanic Technol.*, **31**, 287–301, <https://doi.org/10.1175/JTECH-D-12-00119.1>.
- Yu, H. Z., H. L. Wang, Z. Y. Meng, M. Mu, X. Y. Huang, and X. Zhang, 2017: A WRF-Based tool for forecast sensitivity to the initial perturbation: The conditional nonlinear optimal perturbations versus the first singular vector method and comparison to MM5. *J. Atmos. Oceanic Technol.*, **34**, 187–206, <https://doi.org/10.1175/JTECH-D-15-0183.1>.
- Zhang, Z., and T. N. Krishnamurti, 1997: Ensemble forecasting of hurricane tracks. *Bull. Amer. Meteor. Soc.*, **78**(12), 2785–2796, [https://doi.org/10.1175/1520-0477\(1997\)078<2785:EFOHT>2.0.CO;2](https://doi.org/10.1175/1520-0477(1997)078<2785:EFOHT>2.0.CO;2).
- Zhao, Y., and B. Wang, 2008: Numerical experiments for typhoon Dan incorporating AMSU-A retrieved data with 3DVM. *Adv. Atmos. Sci.*, **25**(4), 692–703, <https://doi.org/10.1007/s00376-008-0692-2>.
- Zhao, Y., B. Wang, and Y. Wang, 2007: Initialization and simulation of a landfalling typhoon using a variational bogus mapped data assimilation (BMDA). *Meteor. Atmos. Phys.*, **98**, 269–282, <https://doi.org/10.1007/s00703-007-0265-4>.
- Zhao, Y., B. Wang, and J. J. Liu, 2012: A DRP-4DVar data assimilation scheme for typhoon initialization using sea level pressure data. *Mon. Wea. Rev.*, **140**, 1191–1203, <https://doi.org/10.1175/MWR-D-10-05030.1>.
- Zhou, F. F., and M. Mu, 2011: The impact of verification area design on tropical cyclone targeted observations based on the CNOP method. *Adv. Atmos. Sci.*, **28**(5), 997–1010, <https://doi.org/10.1007/s00376-011-0120-x>.
- Zhou, F. F., and M. Mu, 2012: The impact of horizontal resolution on the CNOP and on its identified sensitive areas for tropical cyclone predictions. *Adv. Atmos. Sci.*, **29**(1), 36–46, <https://doi.org/10.1007/s00376-011-1003-x>.
- Zhou, F. F., M. Yamaguchi, and X. H. Qin, 2016: Possible sources of forecast errors generated by the global/regional assimilation and prediction system for landfalling tropical cyclones. Part I: Initial uncertainties. *Adv. Atmos. Sci.*, **33**(7), 841–851, <https://doi.org/10.1007/s00376-016-5238-4>.
- Zou, X., F. Vandenberghe, M. Pondecà, and Y. H. Kuo, 1997: Introduction to adjoint techniques and the MM5 adjoint modeling system. NCAR Technical Note NCAR/TN-435+STR, 117 pp, <https://doi.org/10.5065/D6F18WNN>.